Journal of Earth Science, *Vol. 30*, *No. 1*, *p. 37–51*, *February 2019* *ISSN 1674-487X*
Printed in China
https://doi.org/10.1007/s12583-018-0863-8

Geochronology and Petrochemistry of Volcanic Rocks in the Xaignabouli Area, NW Laos

Meifeng Shi*, Zhenbo Wu, Shusheng Liu, Zhimin Peng, Linnan Guo, Fei Nie, Siwei Xu
Chengdu Center, *China Geological Survey*, *Chengdu* 610081, *China*
Meifeng Shi: https://orcid.org/0000-0002-1604-3588

ABSTRACT: An integrated study of zircon U-Pb geochronology and petrochemistry, together with zircon Lu-Hf isotopes, has been carried out on the basaltic-andesitic tuff and volcanic breccia from the Nam Hang Formation and andesitic tuff from the Muang-Nan Formation in the Xaignabouli area, which had been mapped as the Permian–Early Triassic on the 1 : 1 000 000 geological map or Late Carboniferous on the 1 : 200 000 geological maps. Zircon U-Pb dating of three samples yielded weighted mean ages of 235±2.6, 232±1.4 and 278±2.8 Ma, respectively, suggesting a Late Triassic origin for the Nam Hang Formation and an Early Permian origin for the Muang-Nan Formation. Geochemically, they are characterized by depletions in HFSEs (e.g., Nb, Ta, Ti) and high LILE/HFSE ratios, and they have positive zircon $\varepsilon_{Hf}(t)$ values of 8.7–15.9, which exhibits the continental arc volcanic affinity and partial melting of subducting oceanic slab in the magma source. Combined with spatial occurrence of the volcanic rock and existing geochronological and geochemical data, we suggest that the Xaignabouli-Luang Prabang volcanic belt can be linked to the Loei-Phetchabun belt. The Permian–Triassic volcanic rocks in this belt might be a product of the Nan back-arc basin eastward subduction.
KEY WORDS: volcanic rock, zircon U-Pb geochronology, geochemistry, zircon Lu-Hf isotope, Xaignabouli, Laos.

0 INTRODUCTION

The tectonics of the Indochina Peninsula consists of a collage of continental blocks, e.g., Sibumasu, Indochina and South China blocks, which are separated by the Changning-Menglian-Chiang Mai-Bentong-Raub suture, the Jinshajiang-Ailaoshan-Song Ma suture (Fig. 1a; Faure et al., 2014; Roger et al., 2014; Metcalfe, 2013, 2011; Liu et al., 2012; Sone and Metcalfe, 2008; Hutchison, 1989). The spatial-temporal relationships of widely developed Paleozoic to Mesozoic volcanic belts are significant to the Paleotethyan tectonic evolution research, such as the Loei belt, Luang Prabang-Xaignabouli belt, Phetchabun belt, Truong Son belt and Nan-Sa Kaeo suture in the Indochina Block. The present study mainly focuses on the Nan suture, Loei and Phetchabun volcanic belt (Thassanapak et al., 2017; Wang et al., 2017; Yang et al., 2016; Salam et al., 2014; Zaw et al., 2014; Panjasawatwong et al., 2006; Intasopa and Dunn, 1994; Intasopa, 1993), while there are few reports about the Petro-stratigraphic and tectonic settings of northwestern Laos (Qian et al., 2016a, b, 2015; Rossignol et al., 2016; Blanchard et al., 2013; Stokes et al., 1996) due to the lack of detailed geological survey work and large-scale geological maps.

The Loei belt is constrained by the western Nan-Sa Kaeo suture, and may extend from western Cambodia up through Sa Kaeo, Phetchabun and the Loei Province in Thailand into NW Laos. The Loei belt contains multiple generations of successive arc-related magmatic events, including Silurian rhyolite (U-Pb zircon: ca. 434–428 Ma; Zaw and Meffre, 2007), Devonian–Carboniferous arc basalt/andesite (Rb/Sr age: 374–361 Ma; Panjasawatwong et al., 2006; Intasopa and Dunn, 1994), mid-Carboniferous volcanogenic sedimentary sequence (U-Pb zircon: 327±7 Ma; Zaw and Meffre, 2007), Late Carboniferous intrusive rocks (U-Pb zircon: 310±8 Ma; Salam et al., 2014; Zaw and Meffre, 2007), Late Permian–Earliest Triassic and Middle Triassic arc basaltic-rhyolitic rocks (U-Pb zircon: ca. 254–241 and 228 Ma; Kamvong et al., 2014; Salam et al., 2014; our unpublished data). In Laos, from Luang Prabang to Xaignabouli and Pak Lay belt, the existing data show that the Triassic (especially Late Triassic) basaltic-andesitic and volcanoclastic rocks are extensively developed (K-Ar: 210–227 Ma; U-Pb zircon: 215–250 Ma; Qian et al., 2016b; Rossignol et al., 2016; Blanchard et al., 2013; Stokes et al., 1996), the Carboniferous mafic, andesitic, rhyolitic rocks have also been reported in Luang Prabang and Muang Feuang (southeast of Xaignabouli) area (U-Pb zircon: 304–350 Ma; Qian et al., 2016a, 2015). However, the relationships between the Luang Prabang-Xaignabouli belt and the Loei and Phetchabun belt are poorly defined.

Based on the latest 1 : 200 000 geological mapping results finished by Chengdu Center of China Geological Survey, combined with geochronology, petrochemistry and zircon Hf isotopic analysts of the volcanic rocks from the Nam Hang Formation and overlying (?) Muang-Nan Formation, this paper aims

*Corresponding author: shimeifeng-1204@163.com

Manuscript received June 9, 2018.
Manuscript accepted October 18, 2018.

Shi, M. F., Wu, Z. B., Liu, S. S., et al., 2019. Geochronology and Petrochemistry of Volcanic Rocks in the Xaignabouli Area, NW Laos. *Journal of Earth Science*, 30(1): 37–51. https://doi.org/10.1007/s12583-018-0863-8. http://en.earth-science.net

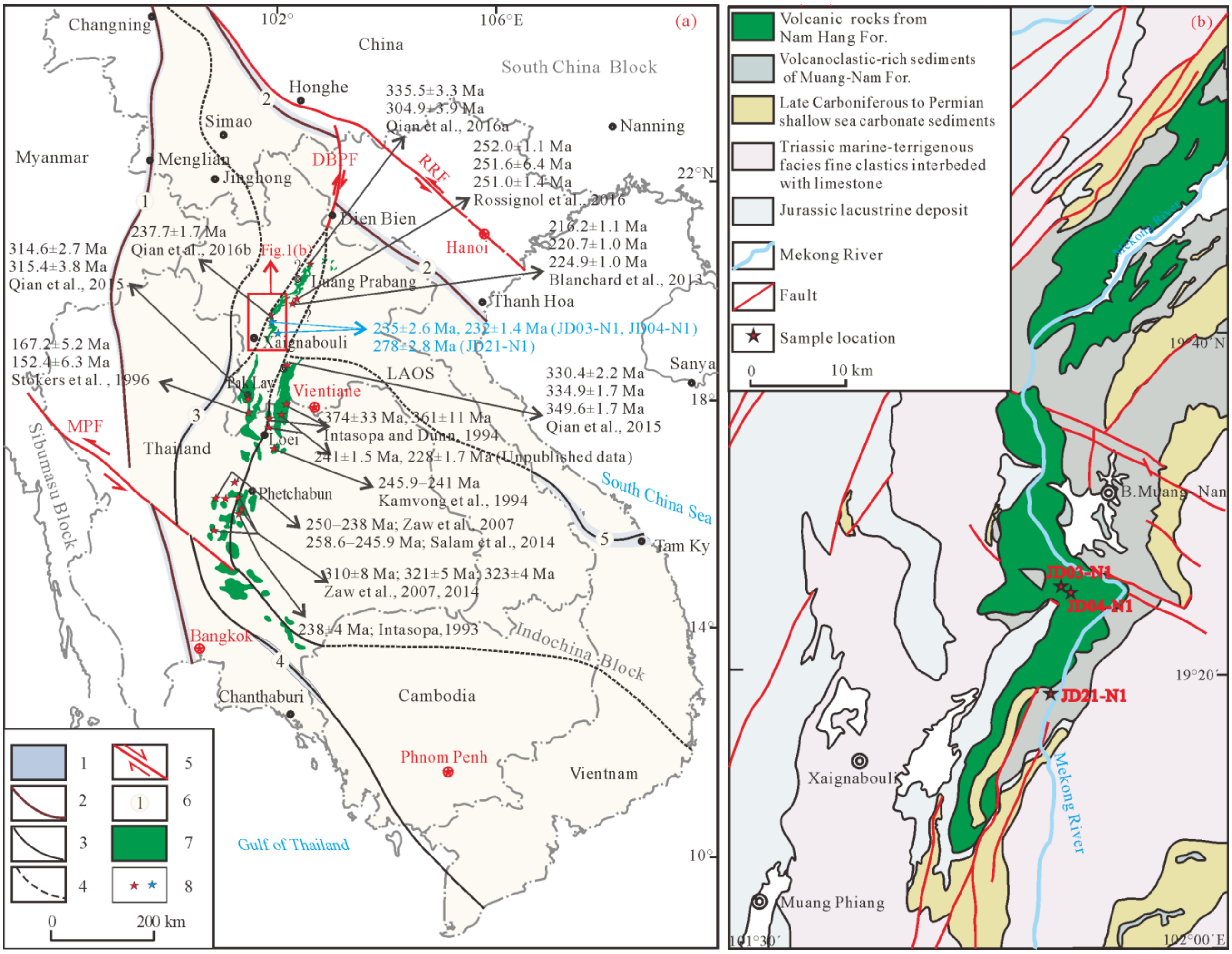

Figure 1. (a) Tectonic map and distribution of the volcanic belts in NW Laos and NE Thailand (modified from Shi et al., 2015; Qian et al., 2015; Metcalfe, 2013); (b) simplified geological map of Xaignabouli area. 1. Ophiolitic melange belt; 2. boundary for Indochina Block; 3. sub-tectonic boundary; 4. speculated boundary; 5. large strike-slip faults; 6. suture zones: ① Changning-Menglian-Chiang Mai suture zone, ②Ailaoshan-Song Ma suture zone, ③ Nan suture zone, ④ Sa Kaeo suture zone, ⑤ Tamky-Phuoc Son suture zone; 7. distribution of the volcanic belts; 8. collected and analyzed age data. RRF. Red River fault; DBPF. Dien Bien Phu fault; MPF. Mae Ping fault.

at probing the connection of Luang Prabang-Xaignabouli belt and Loei-Phetchabun belt, and to improve our understanding of the tectonic evolution of northwestern Laos.

1 GEOLOGICAL SETTING AND PETROGRAPHY

According to our latest geological survey results, sixteen lithostratigraphic units are established in the Xaignabouli area, including the pre-Carboniferous felsic high greenschist-low amphibolite facies schist; Lower Carboniferous Silang Formation lithic feldspathic sandstone; Upper Carboniferous Nam Hang Formation basalt, basaltic andesite, volcanic breccia, and basaltic-andesitic tuff display a significant characteristic of eruption rhythms (mapped as Permian–Early Triassic sequences on the 1 : 1 000 000 geological map; DGM, 1990); and Muang-Nan Formation siltstone, mudstone with basaltic-andesitic tuff interlayers, silicalite; Late Carboniferous to Permian fossils-rich limestone; Triassic marine-terrigenous detrital sequence with limestone layers, Jurassic–Cretaceous lacustrine sediments and Neogene coal-bearing lacustrine-limnetic sediments.

The Nam Hang Formation and the Muang-Nan Formation formed the Muang-Nan anticlinorium in the Xaignabouli area, no bottom exposed and conformable contact is clear between the two formations. The tuffaceous siltstones from the Upper Muang-Nan Formation contain brachiopods *Crurithyris* sp. and *Neochonetes* sp. Meanwhile, the fossil *Profusulinella* sp. is collected at the bottom of the Upper Carboniferous–Lower Permian Don Kaeo Formation limestone, which is one of the index fossils of the Late Carboniferous, where the limestone conformably overlies on the Muang-Nan Formation in Ban Hang of the Xaignabouli District. Accordingly, both Nam Hang Formation and Muang-Nan Formation are assigned to the Late Carboniferous (Fig. 2; Wu et al., 2017). However, Qian et al. (2016b) reported a zircon U-Pb age of 237.7 Ma of the basaltic-andesite from the riverside of the Mekong River near the Xaignabouli City. To strictly constrain the eruption age of the volcanic rocks and tectonic setting, two samples (JD03-N1, JD04-N1) from the Nam Hang Formation and one sample (JD21-N1) from the Muang-Nan Formation are collected for zircon U-Pb dating and Lu-Hf isotopic analyses respectively and relevant eight fresh samples for major elements, trace elements and REE analyses.

Sample JD03-N1 and sample JD04-N1 are taken from Nam Hang Formation on the western side of Mekong Bridge along the road from Xaignabouli to B.Muang-Nan (Fig. 1b; Figs. 3a, 3b). On this section, the outcrops are composed of the dark-grey olivine-phyric basalt, augite-phyric basalt, amygdaloidal basalt, basaltic-andesitic tuff and basaltic-andesite interlayers. JD03-N1 (19°25′23″N, 101°50′41″E) is the basaltic-andesitic tuff, mainly composed of breccia and tuffaceous matrix (Figs. 3a, 3d). The breccia content (ca. 20%–25%) includes angular andesite, basalt, and amygdaloidal basalt debris and clinopyroxene phenocrysts, with 2–5 mm in long axis, and the tuffaceous matrix consists of the phenocrysts of plagioclase and clinopyroxene, and the lithic debris (75%–80%) of andesite, basalts. Plagioclases are replaced by sericite and prehnite, clinopyxenes are partly replaced by chlorite, and some of them enclosed magnetite, zircon and apatite. JD04-N1 (19°25′33″N, 101°50′50″E) is basaltic-andesitic volcanic breccia (Figs. 3b, 3e), mainly composed of angular amygdaloidal andesitic-basaltic breccia (80%–85%) and tuff (15%–20%). The breccia mostly is 20–40 mm in long axis. Some calcite veins are developed along the lithic fissures.

Sample JD21-N1 (19°18′37″N, 101°49′41″E) is taken from the Muang-Nan Formation along the road from Xaignabouli to the Thai Hydropower Station (Fig. 1b), and here the conformable contact between the Nam Hang Formation and Muang-Nan Formation is clear (Fig. 3c). JD21-N1 is a cataclastic andesitic breccia-bearing tuff, outcrops as interlayers with sandy siltstone and siliceous siltstone. The lithology is mainly andesitic, amygdaloidal andesitic breccia (25%–30%, 2–5 mm in long axis) and plagioclase phenocrysts (approximately 3%–5%, 0.1–0.5 mm in long axis) and andesitic lithic-debris (65%–70%, 1–2 mm in long axis) (Fig. 3f), plagioclase is replaced by sericites and mineral lineation is partly developed of sericite.

2 ANALYTICAL METHODS

Zircons were separated and cast in an epoxy mount, and polished to select the grains for analysis. Zircons were documented with transmitted and reflected light micrographs and cathodoluminescence (CL) images, using scanning electron microscope of FEI Quanta 400 FEG in the Hebei Institute of Regional Geological Survey, China. Zircon U-Pb dating was carried out by LA-ICP-MS at Beijing Geo Analysis Technology Co., Ltd. The laser beam spot diameter is 32 μm. Helium was used as the carrier gas, zircon GJ1 as an external standard, and the analysis method and instrument parameters were described by Hou et al. (2009). The isotope ratio of analyzed spots, individual U-Pb age, and U-Th-Pb contents were calculated using ICPMS DataCal (Liu et al., 2010). All analyzed zircon grains show the low signal of common ^{204}Pb and high ^{206}Pb/^{204}Pb ratios, so common Pb correction was not necessary. The Isoplot/Ex_ver3 was used for the weighted mean age calculation and concordia diagrams making.

Zircon *in situ* Lu-Hf isotopes analysis was performed on an ESI NWR193 laser ablation microprobe instrument linked with a Neptune plus multi-collector ICP-MS at Beijing Geo Analysis Technology Co., Ltd. The analysis method was similar to that of Wu et al. (2006). The laser beam spot diameter is 40 μm. The isobaric interference correction was undertaken to calculate the ^{176}Lu/^{177}Hf and ^{176}Hf/^{177}Hf ratios using ^{176}Lu/^{175}Lu=0.026 58 and ^{176}Yb/^{173}Yb=0.796 218 (Chu et al, 2002). The reference standards for our normal analyses used zircon GJ1, which has a weighted mean ^{176}Hf/^{177}Hf ratio of 0.282 007±0.000 007 (2σ, n=36). In order to correct the

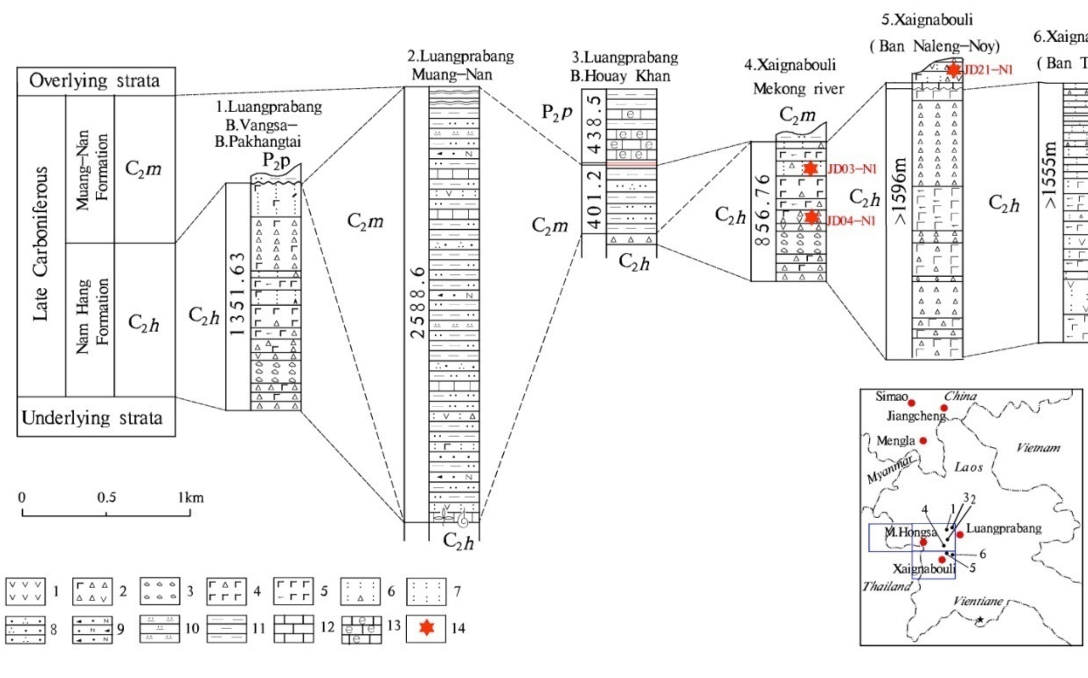

Figure 2. Stratigraphic columnar correlation of volcanic-sedimentary strata in the Xaignabouli and adjacent areas. 1. Andesite; 2. basaltic-andesitic volcanic breccia; 3. volcanic agglomerate; 4. volcanic breccia-bearing basalt; 5. augite-phyric basalt; 6. volcanic breccia-bearing tuff; 7. tuff; 8. quartz sandstone; 9. lithic arkose; 10. silicalite; 11. mudstone; 12. limestone; 13. bioclastic limestone; 14. sampling layer.

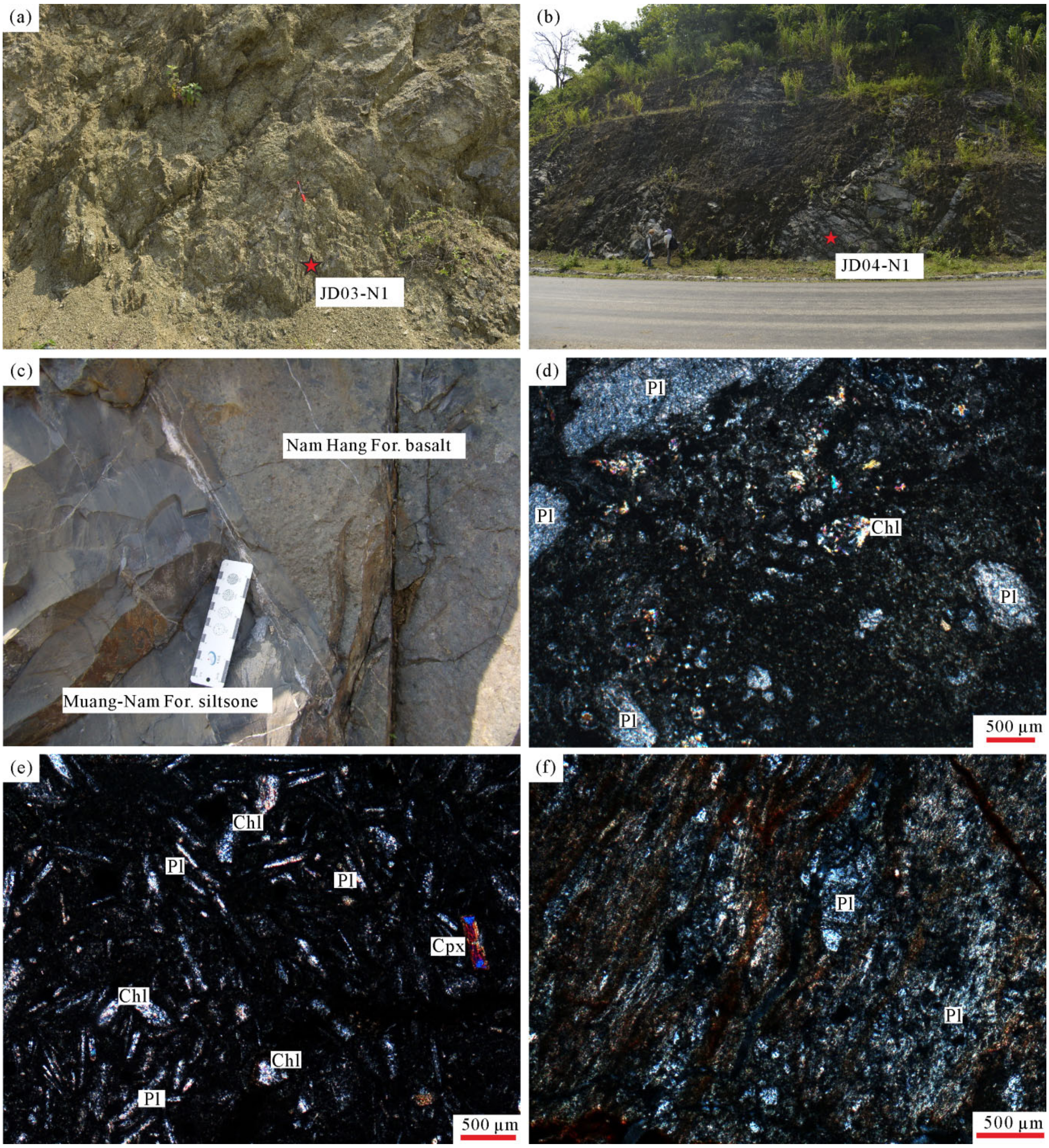

Figure 3. Field photos and microscopic photographs for the volcanic rocks in the Xaignabouli area. (a) (d) basaltic-andesitic tuff; (b) (e) basaltic-andesitic volcanic breccia; (c) conformable contact between Nam Hang Fm. and Muang-Nan Fm.; (f) andesitic breccia-bearing tuff. Pl. Plagioclase; Chl. chlorite; Cpx. Clinopyroxene; Fm. formation.

instrumental quality deviation, the Yb isotope ratios were normalized to $^{172}Yb/^{173}Yb$=1.352 74 and the Hf isotope ratios to $^{179}Hf/^{177}Hf$=0.732 5 using an exponential law (Chu et al., 2002).

Eight samples were crushed below 200 mesh under non-pollution condition for major and trace elements analysis. Both major and trace elements analysis was completed at the State Key Laboratory of Geological Processes and Mineral Resources, China University of Geosciences in Wuhan. The main elements were analyzed by X-ray fluorescence spectrometry (XRF) and the trace elements were analyzed by inductively coupled plasma mass spectrometry (ICP-MS). The analysis accuracy of major elements is better than 5%, and analysis of trace elements is better than 8%.

3 RESULTS

3.1 Zircon U-Pb Dating and Lu-Hf Isotopic Composition

CL images show that the zircon grains from the basaltic-andesitic tuff (JD03-N1) are euhedral, transparent and display igneous overgrowth (Fig. 4a). Twenty-seven analyses give Th content of 69–2 838 ppm and U content of 84–3 850 ppm, with Th/U=0.1–1.6. Eight analyses had a large error which wasn't calculated here. Twelve analyses yielded a weighted mean age of 235±2.6 Ma with MSWD=1.7 (Fig. 4b, Table 1). This age is interpreted as the crystallization age of the basaltic-andesitic

Table 1 LA-ICP-MS zircon U-Pb data of the volcanic rocks from Xaignabouli area, NW Laos

Spot No.	Concentration		Th/U	Isotopic ratio						Calculated apparent age (Ma)					
	Th	U		$^{207}Pb/^{206}Pb$		$^{207}Pb/^{235}U$		$^{206}Pb/^{238}U$		$^{207}Pb/^{206}Pb$		$^{207}Pb/^{235}U$		$^{206}Pb/^{238}U$	
	(ppm)			Ratio	1σ	Ratio	1σ	Ratio	1σ	Age	1σ	Age	1σ	Age	1σ
JD03-N1-01	335	536	0.62	0.050 92	0.000 63	0.259 53	0.004 31	0.036 95	0.000 38	235	28	234	3	234	2
JD03-N1-02	94	762	0.12	0.050 33	0.000 58	0.253 91	0.004 35	0.036 60	0.000 50	209	26	230	4	232	3
JD03-N1-03	255	1093	0.23	0.050 01	0.000 57	0.258 10	0.004 41	0.037 45	0.000 51	195	26	233	4	237	3
JD03-N1-06	325	276	1.18	0.062 34	0.001 74	0.568 96	0.010 96	0.067 33	0.001 50	687	55	457	7	420	9
JD03-N1-07	213	723	0.29	0.050 58	0.000 64	0.259 71	0.004 34	0.037 26	0.000 44	220	30	234	4	236	3
JD03-N1-09	509	1032	0.49	0.050 22	0.001 12	0.252 25	0.006 68	0.036 44	0.000 57	206	52	228	5	231	4
JD03-N1-11	94	162	0.58	0.051 45	0.001 24	0.296 93	0.006 99	0.042 07	0.000 57	261	53	264	5	266	4
JD03-N1-12	2838	3850	0.74	0.050 00	0.000 69	0.248 82	0.003 88	0.036 13	0.000 56	195	36	226	3	229	3
JD03-N1-13	105	191	0.55	0.050 57	0.001 12	0.291 74	0.007 64	0.041 86	0.000 59	220	52	260	6	264	4
JD03-N1-15	208	1451	0.14	0.050 48	0.000 56	0.254 53	0.003 77	0.036 61	0.000 51	217	26	230	3	232	3
JD03-N1-16	69	208	0.33	0.049 66	0.001 36	0.181 11	0.005 90	0.026 49	0.000 48	189	60	169	5	169	3
JD03-N1-20	412	667	0.62	0.050 78	0.000 67	0.260 03	0.006 05	0.037 12	0.000 76	232	31	235	5	235	5
JD03-N1-21	722	1776	0.41	0.050 46	0.000 77	0.252 49	0.006 06	0.036 24	0.000 60	217	31	229	5	229	4
JD03-N1-23	195	120	1.62	0.053 62	0.001 47	0.406 56	0.010 83	0.055 03	0.000 62	354	58	346	8	345	4
JD03-N1-24	170	241	0.70	0.065 19	0.000 70	1.104 09	0.017 91	0.122 78	0.001 56	789	217	755	9	747	9
JD03-N1-25	502	1997	0.25	0.050 54	0.000 54	0.260 53	0.004 52	0.037 43	0.000 66	220	24	235	4	237	4
JD03-N1-26	91	84	1.09	0.073 51	0.001 88	1.332 61	0.035 17	0.131 69	0.001 74	1028	52	860	15	797	10
JD03-N1-28	149	227	0.66	0.049 84	0.001 29	0.260 08	0.008 15	0.037 81	0.000 54	187	64	235	7	239	3
JD03-N1-29	169	229	0.74	0.049 55	0.001 18	0.260 61	0.006 47	0.038 18	0.000 38	176	56	235	5	242	2
JD04-N1-01	253	418	0.60	0.051 09	0.002 82	0.255 03	0.015 41	0.036 17	0.000 59	256	123	231	12	229	4
JD04-N1-02	147	695	0.21	0.060 36	0.000 74	0.631 99	0.012 52	0.075 89	0.001 21	617	26	497	8	472	7
JD04-N1-03	167	225	0.74	0.050 36	0.001 52	0.256 30	0.008 11	0.036 94	0.000 54	213	70	232	7	234	3
JD04-N1-04	685	860	0.80	0.052 95	0.000 81	0.267 50	0.004 99	0.036 61	0.000 37	328	31	241	4	232	2
JD04-N1-05	212	357	0.59	0.051 58	0.000 89	0.266 42	0.005 51	0.037 47	0.000 54	265	36	240	4	237	3
JD04-N1-06	213	380	0.56	0.051 74	0.000 89	0.261 24	0.006 31	0.036 62	0.000 66	272	44	236	5	232	4
JD04-N1-07	317	477	0.67	0.049 55	0.001 15	0.250 79	0.006 38	0.036 71	0.000 60	172	54	227	5	232	4
JD04-N1-08	449	557	0.81	0.053 12	0.000 92	0.270 28	0.006 09	0.036 88	0.000 59	345	39	243	5	233	4
JD04-N1-09	383	588	0.65	0.056 45	0.001 91	0.282 95	0.013 43	0.036 08	0.000 78	478	74	253	11	229	5

Table 1 Continued

Spot No.	Concentration		Th/U	Isotopic ratio						Calculated apparent age (Ma)					
	Th	U		$^{207}Pb/^{206}Pb$		$^{207}Pb/^{235}U$		$^{206}Pb/^{238}U$		$^{207}Pb/^{206}Pb$		$^{207}Pb/^{235}U$		$^{206}Pb/^{238}U$	
	(ppm)			Ratio	1σ	Ratio	1σ	Ratio	1σ	Age	1σ	Age	1σ	Age	1σ
JD04-N1-10	551	673	0.82	0.055 28	0.000 73	0.279 71	0.007 69	0.036 66	0.000 86	433	30	250	6	232	5
JD04-N1-11	145	189	0.76	0.050 24	0.001 63	0.250 86	0.007 61	0.036 33	0.000 51	206	76	227	6	230	3
JD04-N1-12	262	424	0.62	0.057 90	0.001 80	0.298 31	0.013 80	0.037 25	0.000 98	524	67	265	11	236	6
JD04-N1-13	400	564	0.71	0.052 03	0.000 83	0.260 82	0.006 35	0.036 34	0.000 75	287	37	235	5	230	5
JD04-N1-14	442	519	0.85	0.050 73	0.001 07	0.261 25	0.007 45	0.037 44	0.000 91	228	44	236	6	237	6
JD04-N1-15	307	446	0.69	0.054 32	0.001 50	0.274 67	0.011 40	0.036 58	0.000 92	383	68	246	9	232	6
JD04-N1-16	311	462	0.67	0.050 65	0.000 84	0.259 90	0.005 98	0.037 16	0.000 55	233	37	235	5	235	3
JD04-N1-17	164	307	0.53	0.049 40	0.000 71	0.246 98	0.004 06	0.036 25	0.000 41	165	33	224	3	230	3
JD04-N1-18	289	326	0.89	0.075 10	0.000 91	1.600 54	0.023 21	0.154 63	0.001 92	1072	20	970	9	927	11
JD04-N1-19	520	579	0.90	0.050 70	0.000 85	0.255 66	0.004 53	0.036 64	0.000 52	228	39	231	4	232	3
JD04-N1-21	357	524	0.68	0.050 16	0.001 47	0.255 43	0.008 16	0.036 98	0.000 91	211	101	231	7	234	6
JD04-N1-22	436	624	0.70	0.053 50	0.000 74	0.310 28	0.005 31	0.042 05	0.000 49	350	34	274	4	266	3
JD04-N1-24	166	518	0.32	0.059 55	0.000 86	0.779 82	0.024 97	0.094 91	0.002 71	587	26	585	14	585	16
JD04-N1-25	237	433	0.55	0.051 19	0.000 99	0.261 14	0.005 30	0.037 01	0.000 32	250	44	236	4	234	2
JD04-N1-26	147	282	0.52	0.059 69	0.002 81	0.306 20	0.005 70	0.037 24	0.001 10	591	106	271	4	236	7
JD04-N1-27	414	520	0.80	0.051 81	0.001 26	0.270 26	0.007 83	0.037 85	0.000 76	276	56	243	6	239	5
JD04-N1-28	465	506	0.92	0.058 39	0.001 58	0.293 27	0.009 26	0.036 41	0.000 51	546	64	261	7	231	3
JD04-N1-29	231	409	0.57	0.050 67	0.001 39	0.253 19	0.007 58	0.036 25	0.000 56	233	63	229	6	230	3
JD04-N1-30	381	457	0.83	0.051 58	0.001 72	0.258 14	0.008 52	0.036 40	0.000 46	333	78	233	7	230	3
JD21-N1-01	28	70	0.41	0.058 35	0.003 59	0.352 32	0.021 48	0.044 39	0.000 92	543	103	306	16	280	6
JD21-N1-04	47	115	0.41	0.052 24	0.002 64	0.313 37	0.014 65	0.043 75	0.000 58	295	115	277	11	276	4
JD21-N1-07	60	133	0.45	0.050 87	0.002 49	0.306 72	0.016 36	0.043 66	0.000 54	235	113	272	13	276	3
JD21-N1-08	75	230	0.33	0.051 87	0.001 27	0.315 02	0.007 02	0.044 13	0.000 54	280	56	278	5	278	3
JD21-N1-14	212	419	0.51	0.055 86	0.002 58	0.330 48	0.012 95	0.043 31	0.001 40	456	104	290	10	273	9
JD21-N1-16	34	142	0.24	0.057 48	0.003 20	0.351 62	0.017 80	0.044 58	0.000 60	509	122	306	13	281	4
JD21-N1-18	29	70	0.41	0.050 48	0.002 63	0.310 13	0.014 72	0.044 92	0.000 64	217	122	274	11	283	4
JD21-N1-22	29	60	0.49	0.055 63	0.003 33	0.343 45	0.020 29	0.044 93	0.000 71	439	133	300	15	283	4
JD21-N1-23	85	112	0.75	0.051 67	0.002 45	0.309 41	0.015 14	0.043 42	0.000 62	333	105	274	12	274	4

Table 1 Continued

Spot No.	Concentration		Th/U	Isotopic ratio						Calculated apparent age (Ma)					
	Th	U		$^{207}Pb/^{206}Pb$		$^{207}Pb/^{235}U$		$^{206}Pb/^{238}U$		$^{207}Pb/^{206}Pb$		$^{207}Pb/^{235}U$		$^{206}Pb/^{238}U$	
	(ppm)			Ratio	1σ	Ratio	1σ	Ratio	1σ	Age	1σ	Age	1σ	Age	1σ
JD21-N1-24	41	76	0.54	0.056 51	0.002 58	0.352 24	0.015 65	0.045 34	0.000 69	472	100	306	12	286	4
JD21-N1-26	64	185	0.34	0.057 23	0.001 76	0.338 85	0.010 40	0.042 97	0.000 54	502	69	296	8	271	3
JD21-N1-28	22	54	0.41	0.056 37	0.005 20	0.335 34	0.031 64	0.043 10	0.000 77	478	202	294	24	272	5
JD21-N1-29	79	119	0.67	0.056 33	0.002 61	0.332 38	0.016 36	0.042 77	0.000 90	465	99	291	12	270	6
JD21-N1-34	132	105	1.25	0.054 21	0.002 70	0.332 47	0.017 95	0.044 67	0.001 36	389	111	291	14	282	8

tuff. One grain gives a relatively younger age (167 Ma), while the remaining six analyses give older $^{206}Pb/^{238}U$ ages of 264–797 Ma, which are interpreted as xenocrysts. A total of twenty-eight analyses were performed on twenty-eight zircon grains from sample JD04-N1 (basaltic-andesitic volcanic breccia). The CL images show that most zircons have concentric oscillatory zoning on a patchy zoned core, some display sector zoning (Fig. 4c). The dated grains give the Th and U contents of 147–685 ppm and 695–860 ppm respectively, with the Th/U ratio of 0.21–0.92. The 24 analyses gain a weighted mean age of 232±1.4 Ma with MSWD=0.54 (Fig. 4d, Table 1), which probably represents the volcano eruption time. Other 4 analyses have distinct older ages from 266 to 927 Ma, which are explained as capture zircons. A total of 14 dated spots of 28 zircon grains from JD04-N1 (basaltic-andesitic volcanic breccia) yield $^{176}Yb/^{177}Hf$ and $^{176}Lu/^{177}Hf$ ratios of 0.019 603–0.032 234 and 0.000 844–0.001 371 respectively. In addition, the initial $^{176}Hf/^{177}Hf$ ratios range from 0.282 932 to 0.283 082, with $\varepsilon_{Hf}(t)$ values from +10.5 to +15.9 and single-stage depleted mantle Hf model ages (T_{DM}) varying from 242 to 454 Ma (Fig. 4g; Table 2).

Twenty analyses were carried for sample JD21-N1 (andesitic breccia-bearing tuff), and the CL images show that there are many typical magmatic oscillatory zonings and no inherited cores (Fig. 4e). Six analyses show large error and lower concordance which have not been taken into calculating. The remaining fourteen analyses give the Th and U contents of 22 ppm–212 ppm and 54 ppm–419 ppm respectively, yielding Th/U values varying from 0.24 to 1.25. The concordant 14 data yielded a weighted mean age of 278±2.8 Ma (MSWD=1.3, Fig. 4f; Table 1), which is interpreted as the crystallization age of the andesitic breccia-bearing tuff. Ten grains were selected for Lu-Hf isotopic analysis and yield $^{176}Yb/^{177}Hf$ ratios ranging from 0.018 169 to 0.070 96, $^{176}Lu/^{177}Hf$ ratios from 0.000 859 to 0.002 929 and $^{176}Hf/^{177}Hf$ ratios from 0.282 856 to 0.282 982, with the $f_{Lu/Hf}$= -0.91 to -0.97. The $\varepsilon_{Hf}(t)$ values vary from +8.7 to +13.4 and the Hf-depleted model ages (T_{DM}) from 388 to 570 Ma (Fig. 4g).

3.2 Major and Trace Elements

Major and trace elements contents of 8 samples of volcanic rocks from the Nam Hang Formation and Muang-Nan Formation are listed in Table 3. The results of the analyzed samples give high LOI contents of 4.1–6.7, suggesting that there is some weathering-alteration. Therefore, major oxides normalization is needed (volatile-free), and the following diagrams and descriptions will use the recalculated data. Eight samples have normalized SiO_2 contents ranging from 47.18 wt.% to 61.13 wt.%, with a wide range of MgO from 2.63 wt.% to 19.92 wt.% ($Mg^{\#}$=36–78) and Al_2O_3 from 8.5 wt.% to 20.77 wt.%, and characterized by low TiO_2 from 0.44 wt.% to 1.03 wt.%. Considering the instability of the alkaline elements, the Zr/TiO_2-Nb/Y (Fig. 5a; Winchester and Floyd, 1977) and Th-Co (Fig. 5b; Hastie et al., 2007) classification diagrams are selected for petrology classification, the samples are mainly defined as calc-alkaline or subalkaline andesite/basalt and basaltic andesite.

Volcanic rocks from the Nam Hang Formation and

Muang-Nan Formation generally have similar REE patterns displaying LREE-enrichment, moderately fractionated HREE relative to LREE, with LREE/HREE=3.87–6.3, La_N/Yb_N= 3.38–8.28, δEu=0.9–1.1, without an Eu anomaly (Fig. 5c). In the primitive mantle-normalized spidergram (Fig. 5d), all the basalt and andesitic-basaltic tuff samples characterized by strong depletions in Nb, Ta, Ti and have high LILE/HFSE ratios, consistent with the arc volcanic rocks (Sun and McDonough, 1989).

4 DISCUSSION

4.1 Age of Volcanic Rocks in the Xaignabouli Area

Our data show that the basaltic-andesitic tuff and volcanic breccia from the Nam Hang Formation in the Xaignabouli area have weighted mean ages of 235±2.6 and 232±1.4 Ma respectively, which is consistent with the basaltic-andesite age of 237.7±1.7 Ma (Qian et al., 2016b), marked as the Middle Triassic rather than the Permian–Early Triassic as mapped on the

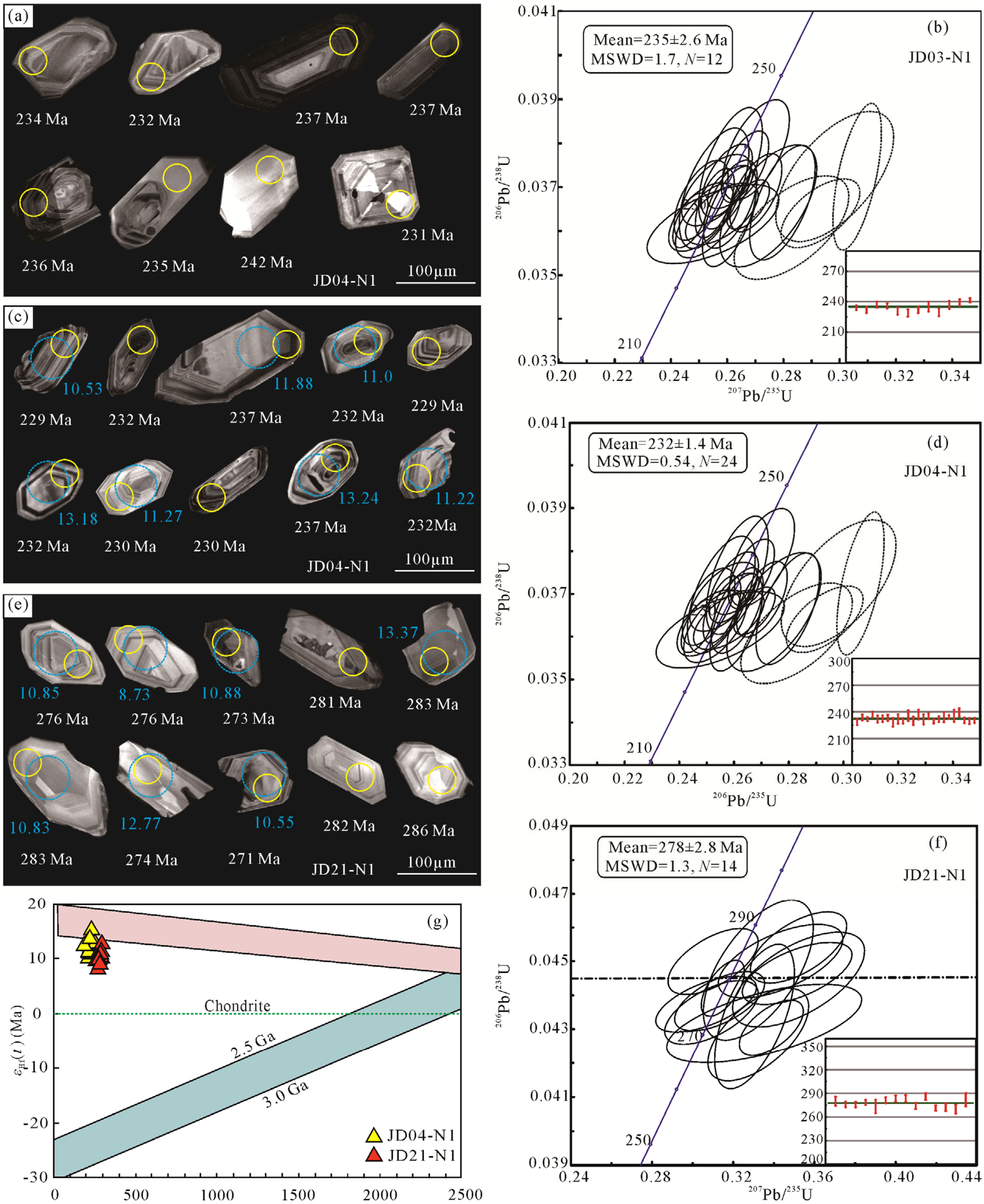

Figure 4. CL images of the representative zircons and LA-ICP-MS zircon U-Pb concordia diagrams and Age (Ma)-$\varepsilon_{Hf}(t)$ diagram for volcanic rocks in the Xaignabouli area. The white and blue circles show the location of zircon U-Pb geochronological analysis and *in situ* Lu-Hf isotopic compositions analysis, respectively.

Table 2 Zircon Lu-Hf isotopic data for volcanic rocks from Xaignabouli area, NW Laos

Analysis	Age (Ma)	$^{176}Hf/^{177}Hf$	2σ	$^{176}Lu/^{177}Hf$	2σ	$^{176}Yb/^{177}Hf$	2σ	$^{176}Hf/^{177}H$ finitial	$\varepsilon_{Hf}(0)$	$\varepsilon_{Hf}(t)$	T_{DM} (Ma)	T_{DM}^{C} (Ma)	$f_{Lu/Hf}$
JD04-N1-1	229.0	0.282 932	0.000 053	0.001 045	0.000 011	0.024 211	0.000 313	0.282 927	5.66	10.53	454.1	588.3	-0.97
JD04-N1-3	233.8	0.282 949	0.000 023	0.001 193	0.000 010	0.027 461	0.000 279	0.282 944	6.26	11.22	431.3	547.9	-0.96
JD04-N1-5	237.1	0.282 965	0.000 022	0.001 064	0.000 006	0.023 527	0.000 144	0.282 961	6.84	11.88	406.9	508.0	-0.97
JD04-N1-6	231.8	0.282 944	0.000 024	0.001 106	0.000 005	0.025 419	0.000 247	0.282 939	6.08	11.00	438.0	560.4	-0.97
JD04-N1-8	233.4	0.283 082	0.000 054	0.001 340	0.000 013	0.032 234	0.000 572	0.283 076	10.96	15.89	242.2	247.3	-0.96
JD04-N1-11	230.0	0.282 951	0.000 025	0.000 844	0.000 019	0.019 603	0.000 443	0.282 948	6.34	11.27	424.2	541.7	-0.97
JD04-N1-14	236.9	0.283 004	0.000 027	0.001 082	0.000 009	0.024 728	0.000 254	0.282 999	8.20	13.24	352.2	420.7	-0.97
JD04-N1-16	235.2	0.282 978	0.000 026	0.001 091	0.000 016	0.025 085	0.000 378	0.282 973	7.27	12.27	389.7	481.5	-0.97
JD04-N1-17	229.5	0.283 037	0.000 034	0.000 961	0.000 014	0.022 472	0.000 685	0.283 032	9.36	14.26	304.5	349.4	-0.97
JD04-N1-19	232.0	0.282 950	0.000 026	0.001 204	0.000 014	0.027 281	0.000 367	0.282 945	6.29	11.21	430.5	547.6	-0.96
JD04-N1-25	234.2	0.282 994	0.000 022	0.001 366	0.000 006	0.031 905	0.000 193	0.282 988	7.87	12.81	368.3	446.4	-0.96
JD04-N1-27	239.5	0.282 986	0.000 024	0.000 959	0.000 020	0.022 191	0.000 476	0.282 981	7.56	12.67	376.8	459.1	-0.97
JD04-N1-29	229.5	0.283 008	0.000 033	0.001 321	0.000 016	0.032 089	0.000 707	0.283 002	8.34	13.18	348.9	418.6	-0.96
JD04-N1-30	230.5	0.283 034	0.000 028	0.001 371	0.000 009	0.031 246	0.000 195	0.283 028	9.26	14.12	311.9	359.4	-0.96
JD21-N1-1	280.0	0.282 897	0.000 024	0.000 859	0.000 008	0.018 169	0.000 196	0.282 893	4.44	10.44	500.6	633.9	-0.97
JD21-N1-4	276.1	0.282 918	0.000 029	0.002 193	0.000 041	0.048 871	0.000 959	0.282 907	5.17	10.85	488.5	604.8	-0.93
JD21-N1-7	275.5	0.282 856	0.000 026	0.001 587	0.000 018	0.033 833	0.000 438	0.282 848	2.96	8.73	570.5	739.6	-0.95
JD21-N1-8	278.4	0.282 952	0.000 033	0.002 054	0.000 020	0.042 607	0.000 580	0.282 941	6.36	12.10	437.7	525.9	-0.94
JD21-N1-14	273.3	0.282 917	0.000 023	0.001 409	0.000 035	0.032 074	0.000 919	0.282 910	5.12	10.88	480.1	600.3	-0.96
JD21-N1-18	283.3	0.282 910	0.000 032	0.001 520	0.000 005	0.032 808	0.000 181	0.282 902	4.88	10.83	491.5	611.5	-0.95
JD21-N1-22	283.3	0.282 982	0.000 029	0.001 507	0.000 013	0.036 042	0.000 333	0.282 974	7.42	13.37	388.1	448.6	-0.95
JD21-N1-23	274.0	0.282 968	0.000 027	0.001 144	0.000 019	0.029 682	0.000 497	0.282 963	6.95	12.77	403.3	479.9	-0.97
JD21-N1-26	271.2	0.282 913	0.000 028	0.002 194	0.000 058	0.048 535	0.001 426	0.282 902	4.97	10.55	496.7	620.1	-0.93
JD21-N1-29	270.0	0.282 884	0.000 031	0.002 929	0.000 007	0.070 960	0.000 193	0.282 869	3.95	9.36	550.4	695.1	-0.91

1 : 1 000 000 geological map (DGM, 1990) or the Upper Carboniferous on the 1 : 200 000 geological map (Wu et al., 2017). Meanwhile, the andesitic tuff from the Muang-Nan Formation yielded a weighted mean age of 278±2.8 Ma, belonging to the Early Permian rather than the Upper Carboniferous as mapped on the 1 : 200 000 geological map (Wu et al., 2017). According to the latest 1 : 200 000 geological survey, no fossils were collected from the Nam Hang Formation, brachiopods fossils (*Crurithyris* sp. and *Neochonetes* sp.) were collected from the tuffaceous siltstones of the Muang-Nan Formation. Generally speaking, the fossils *Crurithyris* sp. appear in the Devonian to the Induan strata (Late Triassic), while the fossils *Neochonetes* sp. occur in the Carboniferous to Permian strata. So there lacks adequate evidence to define the eruption age of the volcanic rocks that are developed in the Xaignabouli area. We suggest that this set of volcanic rocks should be defined as a unique volcanic unit instead of stratigraphic layer.

4.2 Petrogenesis and Tectonic Setting of Volcanic Rocks in the Xaignabouli Area

As described in the previous section, the geochemical samples have been altered to some degree. Hence, we are here just using the incompatible element ratios and Hf isotopic data to discuss the petrogenesis and tectonic setting of the volcanic rocks.

Volcanic rocks from the Nam Hang Formation and Muang-Nan Formation have Mg-numbers of 36–78, and Th content (0.94 ppm–2.01 ppm) is significantly higher than Ta content (0.06 ppm–0.3 ppm) with the Th/Ta ratio of 5–24 (much higher than that of the primitive mantle (1.6), indicative of the arc-like source (Taylor and McLeannan, 1985; Wang et al., 2001). All samples show variable Ba/La (2.63–69.29), Ba/Nb (20.44–170.06) and Ba/Th (14.88–510.35) ratios, and constant $(La/Sm)_N$ (1.58–2.15) (Figs. 6a, and 6b) (Su et al., 2012), which supports significant enrichment of slab-derived fluid in the source and negligible involvement of sediments.

Minor crustal contamination might produce negative Nb-Ta anomalies relative to the LILE and LREE but would result in positive Zr-Hf anomalies due to enrichment of these elements in crustal materials (Zhao et al., 2010). In the primitive mantle-normalized spidergram, all the samples display depletion in Nb-Ta, and the negative Zr-Hf anomalies displayed (Fig. 5d) indicate that little or no crustal contamination occurred. Fourteen zircon grains from the Nam Hang Formation basaltic-andesitic volcanic breccia and ten zircon grains from the Muang-Nan Formation andesitic tuff give a constant $^{176}Hf/^{177}Hf$ ratio of 0.282 932–0.283 082 and 0.282 856–0.282 982, respectively, which means the Hf isotopic have a uniform distribution in the sampling zircons indicating a homogeneous magmatic origin. The positive and wide range $\varepsilon_{Hf}(t)$ values of 8.7–15.9 indicate that their source is mainly depleted mantle or partial melting of subducting oceanic slab (e.g.,

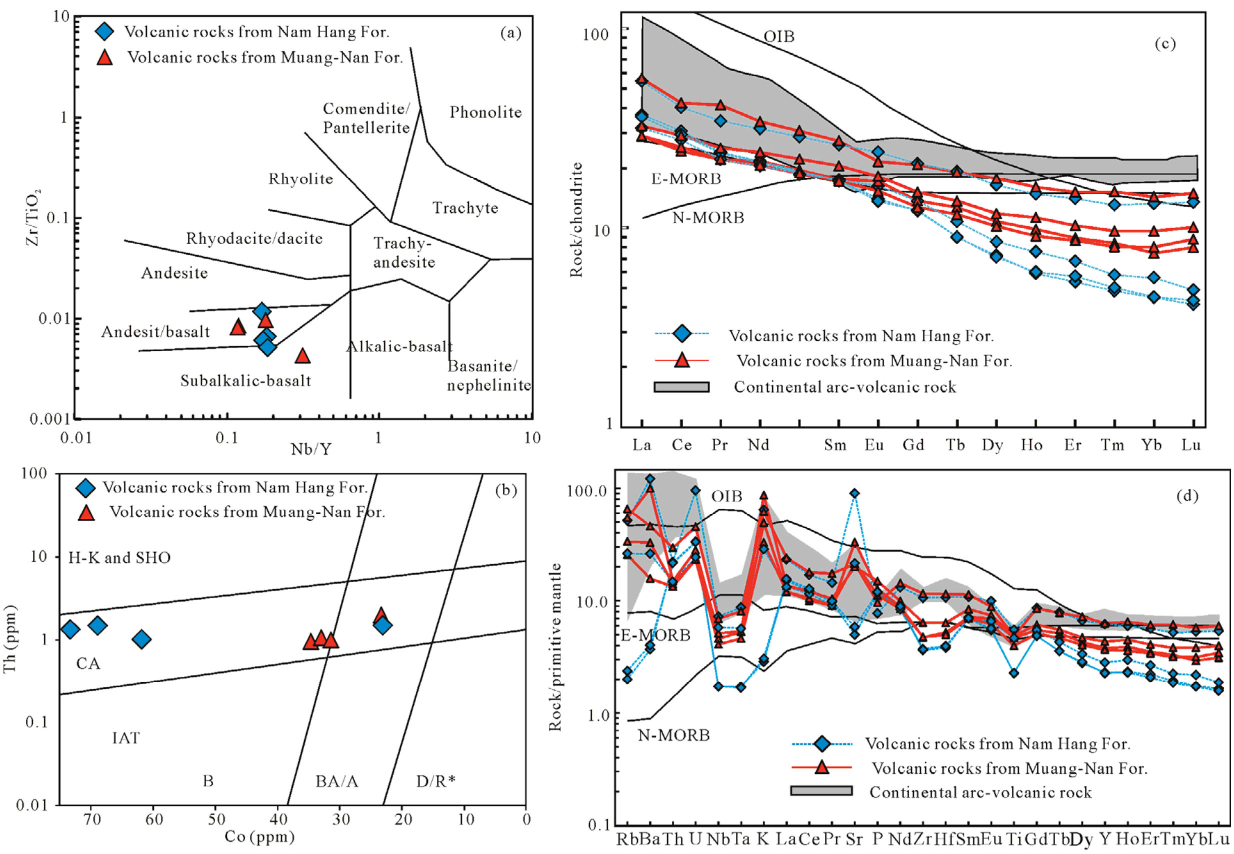

Figure 5. Diagrams for the volcanic rocks in the Xaignabouli area. (a) Nb/Y-Zr/TiO_2 (Winchester and Floyd, 1977); (b) Th-Co classification (Hastie et al., 2007); (c) chondrite-normalized REE patterns; (d) primitive mantle normalized trace element spider. The OIB, E-MORB, N-MORB, normalized values for chondrite and primitive mantle are from Sun and McDonough (1989). CA. calc-alkaline; H-K. high-K calc-alcaline; SHO. shoshonite; IAT. island-arc tholeiite; B. basalt; BA/A. basaltic andesite and andesite; D/R*. dacite and rhyolite (* indicates that latites and trachytes also fall in the D/R fields).

Table 3 Major oxides (wt.%) and trace elements ($\times10^{-6}$) of the volcanic rocks from Xaignabouli area, NW Laos

Sample	Nam Hang Formation				Muang-Nan Formation			
	JD03-h1	JD03-h2	JD03-h3	JD04-h3	JD21-h1	JD21-h2	JD21-h3	JD21-h4
	Basaltic-andesitic tuff			Basalt	Andesitic tuff		Basalt	
SiO_2	45.39	44.10	43.85	50.69	51.77	56.99	48.07	46.99
TiO_2	0.82	0.41	0.41	0.98	0.82	0.84	0.72	0.87
Al_2O_3	10.86	8.14	7.90	17.03	19.36	17.24	17.09	17.57
Fe_2O_3	10.96	10.97	10.67	8.17	10.18	8.89	9.02	9.41
MnO	0.15	0.16	0.16	0.13	0.12	0.14	0.13	0.15
MgO	14.89	18.59	18.52	4.19	3.56	2.46	6.59	6.31
CaO	9.01	10.63	11.01	8.79	2.80	2.61	9.90	9.53
Na_2O	1.16	0.15	0.15	4.21	3.34	2.54	3.28	2.38
K2O	0.65	0.08	0.07	1.45	1.08	1.36	0.76	1.93
P_2O_5	0.20	0.20	0.20	0.14	0.21	0.16	0.19	0.26
LOI	4.90	5.91	6.11	3.78	6.81	6.71	4.10	4.40
$Mg^{\#}$	73	77	78	51	41	36	59	57
SUM	98.99	99.34	99.05	99.55	100.06	99.94	99.84	99.80
Ba	147	24	22	645	183	252	91	535
Rb	13.44	1.34	1.14	25.56	17.00	32.48	13.10	27.09
Sr	368	106	91	1466	557	364	369	344
Y	11.28	9.19	9.32	24.08	14.98	24.46	14.54	17.12
Zr	36.5	35.9	35.5	99.0	45.6	107.9	46.0	60.9
Nb	3.54	1.10	1.10	4.39	2.84	4.20	2.54	3.15
Th	1.03	1.49	1.51	1.52	0.99	2.01	0.94	1.05
U	0.41	0.56	0.56	1.54	0.40	0.75	0.39	0.47
Ta	0.20	0.06	0.06	0.30	0.19	0.28	0.16	0.19
La	7.53	8.78	8.56	12.91	6.86	13.34	6.88	7.73
Ce	16.97	18.79	18.05	24.70	14.93	25.97	15.61	17.82
Pr	2.10	2.29	2.27	3.28	2.10	3.94	2.11	2.40
Nd	9.61	10.15	9.98	14.73	10.16	16.02	9.66	11.23
Hf	1.07	1.06	1.03	2.76	1.39	2.95	1.33	1.68
Sm	2.67	2.63	2.64	4.01	2.69	4.20	2.63	3.15
Eu	0.94	0.81	0.79	1.40	0.99	1.25	0.89	1.06
Gd	2.80	2.50	2.52	4.33	2.81	4.28	2.60	3.11
Tb	0.40	0.34	0.34	0.72	0.48	0.71	0.44	0.51
Dy	2.17	1.85	1.81	4.17	2.74	4.50	2.59	3.00
Ho	0.43	0.34	0.34	0.84	0.56	0.91	0.52	0.64
Er	1.13	0.89	0.95	2.33	1.47	2.51	1.43	1.70
Tm	0.15	0.12	0.13	0.33	0.21	0.39	0.21	0.25
Yb	0.96	0.76	0.77	2.25	1.27	2.43	1.37	1.64
Lu	0.12	0.11	0.11	0.34	0.20	0.38	0.22	0.26
ΣREE	47.98	50.35	49.25	76.33	47.49	80.82	47.14	54.48
LREE	39.83	43.45	42.28	61.02	37.74	64.71	37.77	43.38
HREE	8.15	6.90	6.96	15.31	9.75	16.11	9.37	11.10
LREE/HREE	4.88	6.30	6.07	3.99	3.87	4.02	4.03	3.91
$(La/Yb)_N$	5.64	8.28	8.01	4.11	3.88	3.93	3.61	3.38
$(Th/Nb)_N$	2.4	11.3	11.5	2.9	2.9	4.0	3.1	2.8
δEu	1.05	0.97	0.93	1.03	1.10	0.90	1.04	1.03
δCe	1.05	1.03	1.00	0.93	0.96	0.88	1.01	1.01

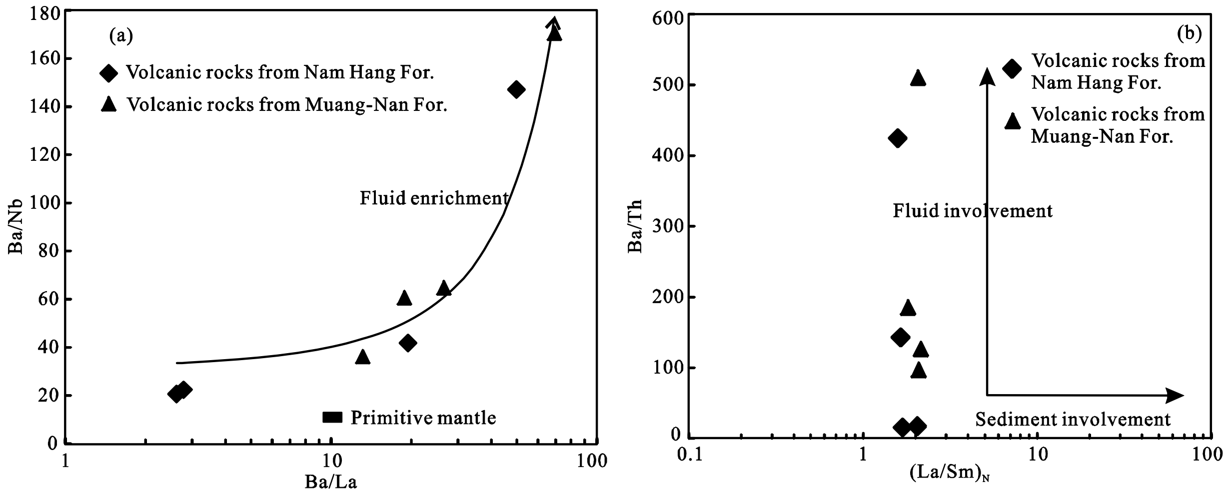

Figure 6. Plots of Ba/La-Ba/Nb (a) and $(La/Sm)_N$-Ba/Th (b) (Su et al., 2012) for the volcanic rocks from the Xaignabouli area.

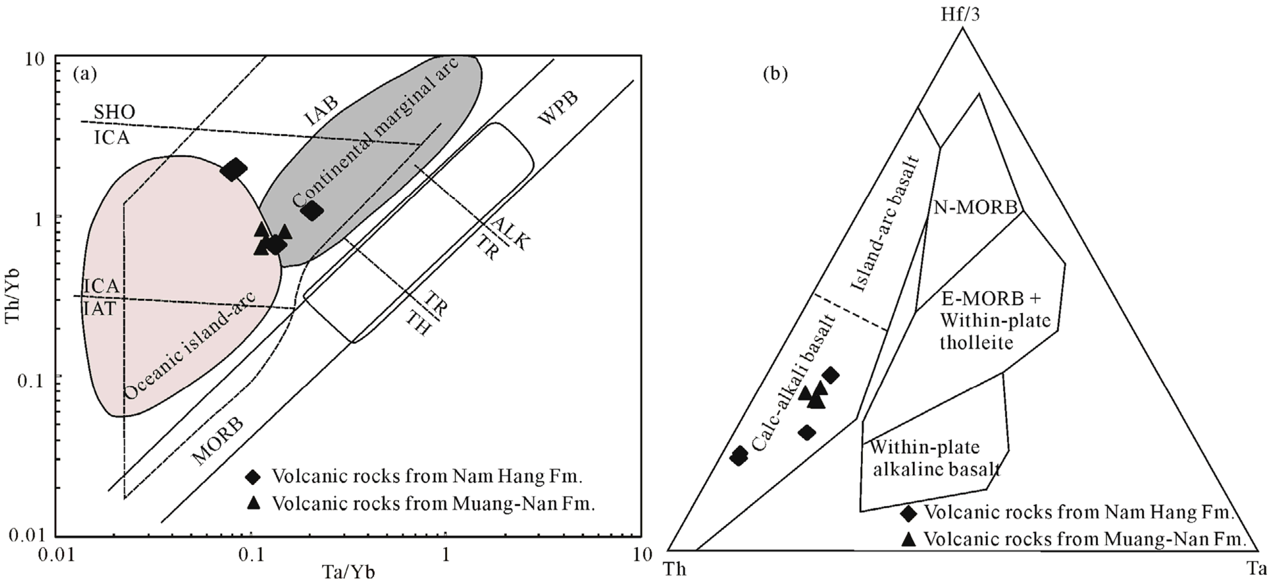

Figure 7. Geochemical discrimination diagrams for the volcanic rocks from the Xaignabouli area. (a) Ta/Yb-Th/Yb (Winchester and Floyd, 1977); (b) Hf/3-Th-Ta (Wood, 1979). IAT. Island-arc tholeiite; ICA. island cal-alkali arc; SHO. shoshonite; TH. tholeiite; TR. transitional basalt; ALK. alkali basalt; IAB. island-arc basalt.

Pearce and Peate, 1995). Furthermore, all samples have relative higher Ba/Nb (20.44–170.06), La/Nb (2.13–7.97) and lower Nb/Th (0.73–3.43) ratios, supporting the magma from partial melting of subducting oceanic slab, rather than from depleted mantle (Li, 1994).

Considering the arc-like petrochemical characteristics of the volcanic rocks from the Xaignabouli area, we exclude the possibility of a back-arc basin or an oceanic ridge tectonic setting. In the Th/Yb-Nb/Yb plot (Fig. 7a), the samples fall into the field of oceanic island-arc or continental marginal arc setting. In the Hf/3-Th-Ta diagram (Fig. 7b), meanwhile, all the samples fall in the field of an island cal-alkali arc setting. Our samples have the Th/Hf ratio of 0.55–1.47, Ta/Hf ratio of 0.06–0.18, and the $Th \cdot Ta/Hf^2$ ratio of 0.06–0.18 which is higher than the primitive mantle ($Th \cdot Ta/Hf^2 = 0.035$) (Wang et al., 2001), so the magma might generate from the continental marginal arc setting.

4.3 Tectonic Implications

Due to a low degree of large-scale geological survey and high-precision geochronology and geochemical data, the tectonic correlation and evolution are poorly defined in the northwestern Indochina Block, especially the extension of the Nan suture and the Loei belt (Wang et al., 2017; Qian et al., 2016b; Yang et al., 2016; Kamvong et al., 2014; Zaw et al., 2014; Metcalfe, 2013, 2011, 2006; Sone et al., 2012; Sone and Metcalfe, 2008; Hutchison, 1989). The Nan suture, also named the Nan-Uttaradit belt, characterized by a discontinuous and disrupted ophiolite sequences, has been considered as a remnant after the closure of the Paleotethyan Ocean (Yang et al., 2016, 2009; Hada et al., 1999; Metcalfe, 1999; Hutchison, 1989) or a back-arc basin (Metcalfe, 2013; Sone and Metcalfe, 2008; Ueno and Hisada, 2001) separating the Sukhothai arc from the Indochina Block which existed from the Carboniferous to the Late Triassic. There are two different opinions about the northern extension of the Nan suture, one supports that the Nan suture extends to the Jinghong suture zone (Song et al., 2018; Wang et al., 2017; Shi et al., 2015; Metcalfe, 2013, 2011; Barr and Charusiri, 2011; Sone and Metcalfe, 2008), and the other one supports that this suture through the Luang Prabang belt is linked to the Jinshajiang-Ailaoshan suture (Qian et al., 2016a; Yang et al., 2016; Feng et al., 2005). For its southern extension, it is generally accepted that it connected to the Sa Kaeo suture zone in Southeastern Thailand and to the Cambodia (Wang et al., 2017; Zaw et al., 2014; Sone and Metcalfe, 2008).

The Loei fold/volcanic belt, mainly develop the andesitic-rhyolitic volcanic rocks which abound in porphyry-related copper-gold and epithermal gold mineralization, have a wide age-spectrum with a main cluster of 305–350 and 216–252 Ma (Fig. 1; Qian et al., 2016a, b, 2015; Rossignol et al., 2016; Salam et al., 2014; Zaw et al., 2014; Blanchard et al., 2013; Zaw and Meffre, 2007; and our unpublished data). Qian et al. (2016a) got the zircon U-Pb ages of 336 and 305 Ma for diabase and basalt from Luang Prabang, according to the petrochemical characteristics and positive $\varepsilon_{Nd}(t)$ and $\varepsilon_{Hf}(t)$ values, they proposed that the Carboniferous magma generates from the continental back-arc basin setting, and the Luang Prabang belt extends north to the Ailaoshan suture zone and the south is linked to the Nan suture during the Late Paleozoic. However, during our latest geological survey in the Xaignabouli and M.kenthao districts, we found large-scale gabbro and chert in M.kenthao and M.Pakbeng areas just along the up-stream direction of Nan River, which need ongoing research. Spatially from Lincang in China, to Sukhothai and Chanthaburi in Thailand and the East Malysia volcanic belt display a tectonic affinity of the Permian–Early Triassic continental arc (Peng et al., 2013; Wang et al., 2010; Hennig et al., 2009), and the Permian–Triassic intermediate-mafic volcanic rocks in the Xaignabouli area are geochemically familiar with the volcanic rocks in the Loei and Phetchabun areas (Qian et al., 2016b). Based on the spatial relationship, it is more reasonable that the Nan-Uttaradit suture zone through the M.kenthao-M.Pakbeng in NW Laos is connected to the Jinghong suture in China, and the Xaignabouli-Luang Prabang volcanic belt is linked to the Loei belt. The Permian–Triassic volcanic rocks in the Xaignabouli-Luang Prabang belt might be a partial melting product of eastward subducting of the Nan back-arc basin.

5 CONCLUSIONS

(1) The basaltic-andesitic tuff and volcanic breccia from the Nam Hang Formation in the Xaignabouli area present a Late Triassic origin (235±2.6 and 232±1.4 Ma, respectively), and the andesitic tuff from the Muang-Nan Formation formed in Early Permian (278±2.8 Ma), rather than the Upper Carboniferous as mapped on the 1: 200 000 geological map.

(2) The arc-like characteristics of the volcanic rocks from the Nam Hang Formation and Muang-Nan Formation, combined with the positive zircon $\varepsilon_{Hf}(t)$ values (8.7–15.9) indicate they might generate from partial melting of the subducting oceanic slab in continental margin arc setting.

(3) Synthesizing existing data, we suggest the Permian–Triassic Xaignabouli-Luang Prabang volcanic belt probably extends to the Loei belt in Thailand, in which the volcanic rocks might be a product of Nan back-arc basin eastward subduction.

ACKNOWLEDGMENTS

We appreciate the helpful comments from two anonymous referees to improve an early version of this paper. This study was financially supported by the China Geological Survey (No. 121201010000150013). The final publication is available at Springer via https://doi.org/10.1007/s12583-018-0863-8.

REFERENCES CITED

Barr, S. M., Charusiri, P., 2011. Volcanic Rocks. In: Ridd, M. F., Barber, A. J., Crow, M. J., eds., The Geology of Thailand. Geological Society, London. 415–439

Blanchard, S., Rossignol, C., Bourquin, S., et al., 2013. Late Triassic Volcanic Activity in South-East Asia: New Stratigraphical, Geochronological and Paleontological Evidence from the Luang Prabang Basin (Laos). *Journal of Asian Earth Sciences*, 70/71: 8–26. https://doi.org/10.1016/j.jseaes.2013.02.024

Chu, N. C., Taylor, R. N., Chavagnac, V., et al., 2002. Hf Isotope Ratio Analysis Using Multi-Collector Inductively Coupled Plasma Mass Spectrometry: An Evaluation of Isobaric Interference Corrections. *Journal of Analytical Atomic Spectrometry*, 17(12): 1567–1574. https://doi.org/10.1039/b206707b

DGM, 1990. Lao P.D.R. Geological and Mineral Occurrence Map 1 : 1 000 000. Department of Geology and Mines, Lao P.D.R., Vientiane

Faure, M., Lepvrier, C., Nguyen, V. V., et al., 2014. The South China Block-Indochina Collision: Where, When, and How?. *Journal of Asian Earth Sciences*, 79: 260–274. https://doi.org/10.1016/j.jseaes.2013.09.022

Feng, Q. L., Chonglakmani, C., Helmcke, D., et al., 2005. Correlation of Triassic Stratigraphy between the Simao and Lampang-Phrae Basins: Implications for the Tectonopaleogeography of Southeast Asia. *Journal of Asian Earth Sciences*, 24(6): 777–785. https://doi.org/10.1016/j.jseaes.2004.11.008

Hada, S., Bunopas, S., Ishii, K., et al., 1999. Rift-Drift History and the Amalgamation of Shan-Thai and Indochina/East Malaya Blocks. In: Metcalfe, I., ed., Gondwana Dispersion and Asian Accretion. A.A. Balkema, Rotterdam. 7–87

Hastie, A. R., Kerr, A. C., Pearce, J. A., et al., 2007. Classification of Altered Volcanic Island Arc Rocks Using Immobile Trace Elements: Development of the Th-Co Discrimination Diagram. *Journal of Petrology*, 48(12): 2341–2357. https://doi.org/10.1093/petrology/egm062

Hennig, D., Lehmann, B., Frei, D., et al., 2009. Early Permian Seafloor to Continental Arc Magmatism in the Eastern Paleo-Tethys: U-Pb Age and Nd-Sr Isotope Data from the Southern Lancangjiang Zone, Yunnan, China. *Lithos*, 113(3/4): 408–422. https://doi.org/10.1016/j.lithos.2009.04.031

Hou, K. J., Li, Y. H., Tian, Y. Y., 2009. *In situ* U-Pb Zircon Dating Using Laser Ablation-Multiion Couting-ICP-MS. *Mineral Deposits*, 28(4): 481–492 (in Chinese with English Abstract)

Hutchison, C.S., 1989. Geological evolution of Southeast Asia. Oxford Monographs on Geology and Geophysis Vol. 13. Clarendon Press, Oxford. 368

Intasopa, S. B., 1993. Petrology and Geochronology of the Volcanic Rocks of the Central Thailand Volcanic Belt: [Dissertation]. University of New Brunswick, Fredericton. 1–242

Intasopa, S., Dunn, T., 1994. Petrology and Sr-Nd Isotopic Systems of the Basalts and Rhyolites, Loei, Thailand. *Journal of Southeast Asian Earth Sciences*, 9(1/2): 167–180. https://doi.org/10.1016/0743-9547(94)90073-6

Kamvong, T., Zaw, K., Meffre, S., et al., 2014. Adakites in the Truong Son and Loei Fold Belts, Thailand and Laos: Genesis and Implications for Geodynamics and Metallogeny. *Gondwana Research*, 26(1): 165–184. https://doi.org/10.1016/j.gr.2013.06.011

Li, S. G., 1994. Implications of ε_{Nd}-La/Nb, Ba/Nb, Nb/Th Diagrams to Mantle Heterogeneity—Classification of Island Arc Basalts and Decomposition of EMII Component. *Geochimica*, 23(2): 105–114 (in Chinese with English Abstract)

Liu, J. L., Tran, M. D., Tang, Y., et al., 2012. Permo-Triassic Granitoids in the Northern Part of the Truong Son Belt, NW Vietnam: Geochronology, Geochemistry and Tectonic Implications. *Gondwana Research*, 22(2): 628–644. https://doi.org/10.1016/j.gr.2011.10.011

Liu, Y. S., Gao, S., Hu, Z. C., et al., 2010. Continental and Oceanic Crust Recycling-Induced Melt-Peridotite Interactions in the Trans-North China Orogen: U-Pb Dating, Hf Isotopes and Trace Elements in Zircons from Mantle Xenoliths. *Journal of Petrology*, 51(1/2): 537–571. https://doi.org/10.1093/petrology/egp082

Metcalfe, I., 1999. The Tethys: How Many? How Old? How Wide? Intern Symposium Shallow Tethys, Chiang Mai. 5: 1–15

Metcalfe, I., 2006. Palaeozoic and Mesozoic Tectonic Evolution and Palaeogeography of East Asian Crustal Fragments: The Korean Peninsula in Context. *Gondwana Research*, 9(1/2): 24–46. https://doi.org/10.1016/j.gr.2005.04.002

Metcalfe, I., 2011. Tectonic Framework and Phanerozoic Evolution of Sundaland. *Gondwana Research*, 19(1): 3–21. https://doi.org/10.1016/j.gr.2010.02.016

Metcalfe, I., 2013. Gondwana Dispersion and Asian Accretion: Tectonic and Palaeogeographic Evolution of Eastern Tethys. *Journal of Asian Earth Sciences*, 66: 1–33. https://doi.org/10.1016/j.jseaes.2012.12.020

Panjasawatwong, Y., Zaw, K., Chantaramee, S., et al., 2006. Geochemistry and Tectonic Setting of the Central Loei Volcanic Rocks, Pak Chom Area, Loei, Northeastern Thailand. *Journal of Asian Earth Sciences*, 26(1): 77–90. https://doi.org/10.1016/j.jseaes.2004.09.008

Pearce, J. A., Peate, D. W., 1995. Tectonic Implications of the Composition of Volcanic Arc Magmas. *Annual Review of Earth and Planetary Sciences*, 23(1): 251–285. https://doi.org/10.1146/annurev.ea.23.050195.001343

Peng, T. P., Wilde, S. A., Wang, Y. J., et al., 2013. Mid-Triassic Felsic Igneous Rocks from the Southern Lancangjiang Zone, SW China: Petrogenesis and Implications for the Evolution of Paleo-Tethys. *Lithos*, 168-169: 15–32. https://doi.org/10.1016/j.lithos.2013.01.015

Qian, X., Feng, Q. L., Wang, Y. J., et al., 2016a. Geochronological and Geochemical Constraints on the Mafic Rocks along the Luang Prabang Zone: Carboniferous Back-Arc Setting in Northwest Laos. *Lithos*, 245: 60–75. https://doi.org/10.1016/j.lithos.2015.07.019

Qian, X., Feng, Q. L., Wang, Y. J., et al., 2016b. Petrochemistry and Tectonic Setting of the Middle Triassic Arc-Like Volcanic Rocks in the Sayabouli Area, NW Laos. *Journal of Earth Science*, 27(3): 365–377. https://doi.org/10.1007/s12583-016-0669-5

Qian, X., Feng, Q. L., Yang, W. Q., et al., 2015. Arc-Like Volcanic Rocks in NW Laos: Geochronological and Geochemical Constraints and Their Tectonic Implications. *Journal of Asian Earth Sciences*, 98: 342–357. https://doi.org/10.1016/j.jseaes.2014.11.035

Roger, F., Jolivet, M., Maluski, H., et al., 2014. Emplacement and Cooling of the Dien Bien Phu Granitic Complex: Implications for the Tectonic Evolution of the Dien Bien Phu Fault (Truong Son Belt, NW Vietnam). *Gondwana Research*, 26: 785–801

Rossignol, C., Bourquin, S., Poujol, M., et al., 2016. The Volcaniclastic Series from the Luang Prabang Basin, Laos: A Witness of a Triassic Magmatic Arc?. *Journal of Asian Earth Sciences*, 120: 159–183. https://doi.org/10.1016/j.jseaes.2016.02.001

Salam, A., Zaw, K., Meffre, S., et al., 2014. Geochemistry and Geochronology of the Chatree Epithermal Gold-Silver Deposit: Implications for the Tectonic Setting of the Loei Fold Belt, Central Thailand. *Gondwana Research*, 26(1): 198–217. https://doi.org/10.1016/j.gr.2013.10.008

Shi, M. F., Lin, F. C., Fan, W. Y., et al., 2015. Zircon U-Pb Ages and Geochemistry of Granitoids in the Truong Son Terrane, Vietnam: Tectonic and Metallogenic Implications. *Journal of Asian Earth Sciences*, 101: 101–120. https://doi.org/10.1016/j.jseaes.2015.02.001

Sone, M., Metcalfe, I., 2008. Parallel Tethyan Sutures in Mainland Southeast Asia: New Insights for Palaeo-Tethys Closure and Implications for the Indosinian Orogeny. *Comptes Rendus Geoscience*, 340(2/3): 166–179. https://doi.org/10.1016/j.crte.2007.09.008

Sone, M., Metcalfe, I., Chaodumrong, P., 2012. The Chanthaburi Terrane of Southeastern Thailand: Stratigraphic Confirmation as a Disrupted Segment of the Sukhothai Arc. *Journal of Asian Earth Sciences*, 61: 16–32. https://doi.org/10.1016/j.jseaes.2012.08.021

Song, J. L., Ding J., Wang B. D., et al., 2018. Wenyu Copper (Silver) Deposit Ore-Forming Geological Background, Jingdong County, Yunnan: Geochronology and Geochemistry Evidences from Ore-Bearing Volcanic Rocks.. *Earth Science*, 43(3): 696–715 (in Chinese with English Abstract)

Stokes, R. B., Lovatt Smith, P. F., Soumphonphakdy, K., 1996. Timing of the Shan-Thai-Indochina Collision: New Evidence from the Pak Lay Foldbelt of the Lao PDR. *Geological Society*, *London*, *Special Publications*, 106(1): 225–232. https://doi.org/10.1144/gsl.sp.1996.106.01.14

Su, Y. P., Zheng, J. P., Griffin, W. L., et al., 2012. Geochemistry and Geochronology of Carboniferous Volcanic Rocks in the Eastern Junggar Terrane, NW China: Implication for a Tectonic Transition. *Gondwana Research*, 22(3/4): 1009–1029. https://doi.org/10.1016/j.gr.2012.01.004

Sun, S. S., McDonough, W. F., 1989. Chemical and Isotopic Systematics of Oceanic Basalts: Implications for Mantle Composition and Processes. *Geological Society*, *London*, *Special Publications*, 42(1): 313–345. https://doi.org/10.1144/gsl.sp.1989.042.01.19

Taylor, S. R., McLeannan, S., 1985. The Continental Crust: Composition and Evolution. Blackwell Scientific Publications, Oxford. 54, 209–372

Thassanapak, H., Udchachon, M., Feng, Q. L., et al., 2017. Middle Triassic Radiolarians from Cherts/siliceous Shales in an Extensional Basin in the Sukhothai Fold Belt, Northern Thailand. *Journal of Earth Science*, 28(1): 9–28. https://doi.org/10.1007/s12583-017-0740-x

Ueno, K., Hisada, K. I., 2001. The Nan-Uttaradit-Sa Kaeo Suture as a Main Paleo-Tethyan Suture in Thailand: Is It Real?. *Gondwana Research*, 4(4): 804–806. https://doi.org/10.1016/s1342-937x(05)70590-6

Wang, Y. J., Qian, X., Cawood, P. A., et al., 2017. Closure of the East Paleotethyan Ocean and Amalgamation of the Eastern Cimmerian and Southeast Asia Continental Fragments. *Earth-Science Reviews*. https://doi.org/10.1016/j.earscirev.2017.09.013

Wang, Y. J., Zhang, A. M., Fan, W. M., et al., 2010. Petrogenesis of Late Triassic Post-Collisional Basaltic Rocks of the Lancangjiang Tectonic Zone, Southwest China, and Tectonic Implications for the Evolution of the Eastern Paleotethys: Geochronological and Geochemical Constraints. *Lithos*, 120(3/4): 529–546. https://doi.org/10.1016/j.lithos.2010.09.012

Wang, Y. L., Zhang, C. J. Xiu, S. Z., 2001. Th/Hf-Ta/Hf Identification of Tectonic Setting of Basalts. *Acta Petrologica Sinica*, 17(3): 413–421

(in Chinese with English Abstract)

Winchester, J. A., Floyd, P. A., 1977. Geochemical Discrimination of Different Magma Series and Their Differentiation Products Using Immobile Elements. *Chemical Geology*, 20: 325–343. https://doi.org/10.1016/0009-2541(77)90057-2

Wood, D. A., 1979. A Variably Veined Suboceanic Upper Mantle—Genetic Significance for Mid-Ocean Ridge Basalts from Geochemical Evidence. *Geology*, 7(10): 499–503. https://doi.org/10.1130/0091-7613(1979)7<499:avvsum>2.0.co;2

Wu, F. Y., Yang, Y. H., Xie, L. W., et al., 2006. Hf Isotopic Compositions of the Standard Zircons and Baddeleyites Used in U–Pb Geochronology. *Chemical Geology*, 234(1/2): 105–126. https://doi.org/10.1016/j.chemgeo.2006.05.003

Wu, Z. B., Liu, S. S., Shi, M. F., et al., 2017. The Report on Regional Geological Mapping. The Geological and Geochemical Mapping in Northern Laos by the Cooperation between China and Laos. 1–257

Yang, W. Q., Feng, Q. L., Shen, S. Y., et al., 2009. Permian Radiolarians, Chert and Basalt from the Nan Suture Zone, Northern Thailand. *Earth Science*, 34(5): 743–751 (in Chinese with English Abstract)

Yang, W. Q., Qian, X., Feng, Q. L., et al., 2016. Zircon U-Pb Geochronological Evidence for the Evolution of the Nan-Uttaradit Suture in Northern Thailand. *Journal of Earth Science*, 27(3): 378–390. https://doi.org/10.1007/s12583-016-0670-z

Zaw, K., Meffre, S., 2007. Metallogenic Relations and Deposit-Scale Studies, Final Report: Geochronology, Metallogenesis and Deposit Styles of Loei Fold Belt in Thailand and Laos PDR, ARC Linkage Project, CODES with Industry Partners. University of Tasmania, Hobart

Zaw, K., Meffre, S., Lai, C. K., et al., 2014. Tectonics and Metallogeny of Mainland Southeast Asia—A Review and Contribution. *Gondwana Research*, 26(1): 5–30. https://doi.org/10.1016/j.gr.2013.10.010

Zhao, J. H., Zhou, M. F., Zheng, J. P., 2010. Metasomatic Mantle Source and Crustal Contamination for the Formation of the Neoproterozoic Mafic Dike Swarm in the Northern Yangtze Block, South China. *Lithos*, 115(1/2/3/4): 177–189. https://doi.org/10.1016/j.lithos.2009.12.001